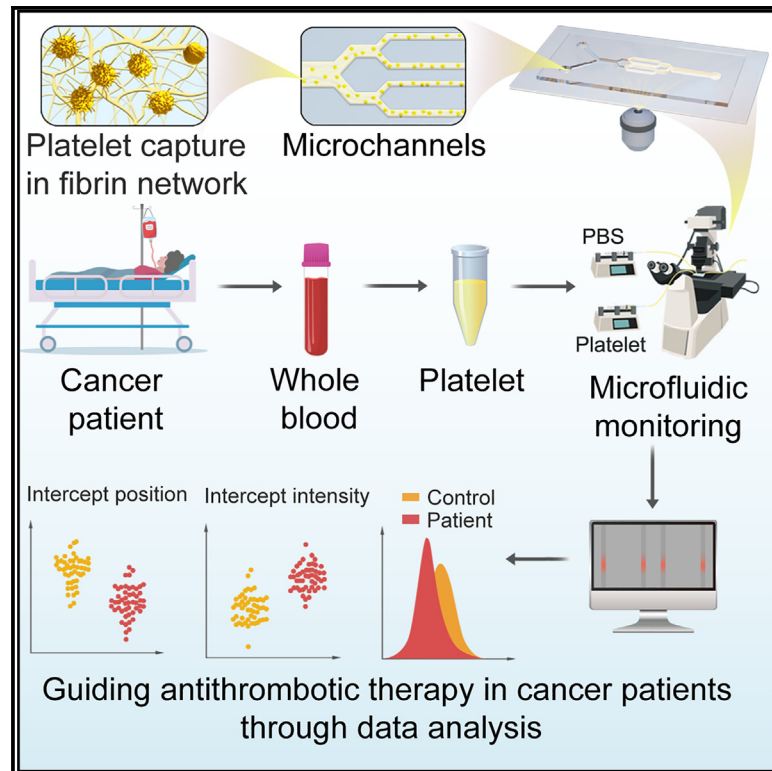


Monitoring circulating platelet activity to predict cancer-associated thrombosis

Graphical abstract



Authors

Bozhao Li, Zefang Lu, Zhenlin Yang, ..., Zhenchuan Song, Guangjun Nie, Suping Li

Correspondence

niegj@nanoctr.cn (G.N.),
lisuping@nanoctr.cn (S.L.)

In brief

Li et al. introduce a microfluidic device that offers a fast, cost-effective method for tracking platelet activation in cancer patients. They demonstrate a strong correlation between elevated platelet activity, tumor progression, and thrombosis risk. This device can help to enable timely and targeted antithrombotic treatment.

Highlights

- A microfluidic device effectively detects tumor-associated platelet hyperactivity
- Platelet activation status is correlated with cancer progression and thrombotic risk
- The device predicts thrombotic events in advanced lung, breast, and liver cancer
- This approach can guide timely antithrombotic therapy in cancer patients



Article

Monitoring circulating platelet activity to predict cancer-associated thrombosis

Bozhao Li,^{1,2,9} Zefang Lu,^{1,2,9} Zhenlin Yang,^{3,9} Xiuping Zhang,⁴ Meiqi Wang,⁵ Tianjiao Chu,¹ Peina Wang,¹ Feilong Qi,^{1,2} Greg J. Anderson,⁶ Ershuai Jiang,¹ Zhenchuan Song,⁵ Guangjun Nie,^{1,2,7,8,*} and Suping Li^{1,2,7,8,10,*}

¹CAS Key Laboratory for Biomedical Effects of Nanomaterials & Nanosafety, CAS Center for Excellence in Nanoscience, National Center for Nanoscience and Technology, Beijing 100190, China

²University of Chinese Academy of Sciences, Beijing 100049, China

³Department of Thoracic Surgery, National Cancer Center/National Clinical Research Center for Cancer/Cancer Hospital, Chinese Academy of Medical Sciences and Peking Union Medical College, Beijing 100021, China

⁴Faculty of Hepato-Biliary-Pancreatic Surgery, Chinese People's Liberation Army (PLA) General Hospital, Institute of Hepatobiliary Surgery of Chinese PLA, Key Laboratory of Digital Hepatobiliary Surgery, PLA, Beijing 100853, China

⁵Breast Center, Fourth Hospital of Hebei Medical University, Shijiazhuang 050035, China

⁶QIMR Berghofer Medical Research Institute, Royal Brisbane Hospital, Brisbane, QLD 4029, Australia

⁷Center of Materials Science and Optoelectronics Engineering, University of Chinese Academy of Sciences, Beijing 100049, China

⁸GBA Research Innovation Institute for Nanotechnology, Guangzhou 510530, China

⁹These authors contributed equally

¹⁰Lead contact

*Correspondence: niegj@nanocr.cn (G.N.), lisuping@nanocr.cn (S.L.)

<https://doi.org/10.1016/j.crmeth.2023.100513>

MOTIVATION Cancer patients often face thrombosis due to platelet hyperactivity, impacting their prognosis. Yet, we lack a simple, sensitive method to analyze their blood coagulation status. To address this concern, our study aims to develop a microfluidic device for detecting platelet activation. It offers improved sensitivity, time-efficient measurements, user-friendly operation, and cost-effective design. This device is envisioned to enhance thrombotic disease management in cancer patients and facilitate more accurate and accessible coagulation analysis in clinical and research settings.

SUMMARY

A characteristic clinical complication in cancer patients is the frequent incidence of thrombotic events. Numerous studies have shown hyperactive/activated platelets to be a critical earlier trigger for cancer-associated thrombus formation. However, there currently is no viable approach to monitor specific changes in tumor-associated platelet activity. Here, we describe a chromatograph-like microfluidic device that is highly sensitive to the activity status of peripheral circulating platelets in both tumor-bearing mice and clinical cancer patients. Our results show a strongly positive correlation between platelet activation status and tumor progression. Six-month follow-up data from advanced cancer patients reveal positive links between platelet activity level and thrombus occurrence rate, with a high predictive capacity of thrombotic events (AUC = 0.842). Our findings suggest that circulating platelet activity status determined by this microfluidic device exhibits sensitive, predictive potential for thrombotic events in cancer patients for directing well-timed antithrombosis treatment.

INTRODUCTION

Cancer-associated thrombotic complications, which can result from both cancer pathology-related factors and cancer therapy-related factors, collectively known as Trousseau syndrome, are the second leading cause of death in cancer patients.^{1–7} The most common thrombosis symptom in cancer patients is deep vein thrombosis (DVT), which occurs in 10%–20% of cancer patients.^{8,9} Although less frequent, arterial thromboembolism is

also reported in 1%–4.7% of cancer patients.^{9,10} These tumor-induced thrombus events actively contribute to tumor metastasis and progression by protecting circulating tumor cells (CTCs) from shear stress and immune surveillance and capturing CTCs at distant organs.^{1,11–15} Furthermore, microthrombi formation in peripheral capillaries and arterioles in the lungs, hearts, and other organs of cancer patients easily leads to patient death because of organ failure. Thus, cancer and coagulation disorders can reciprocally promote pathogenesis, accelerating



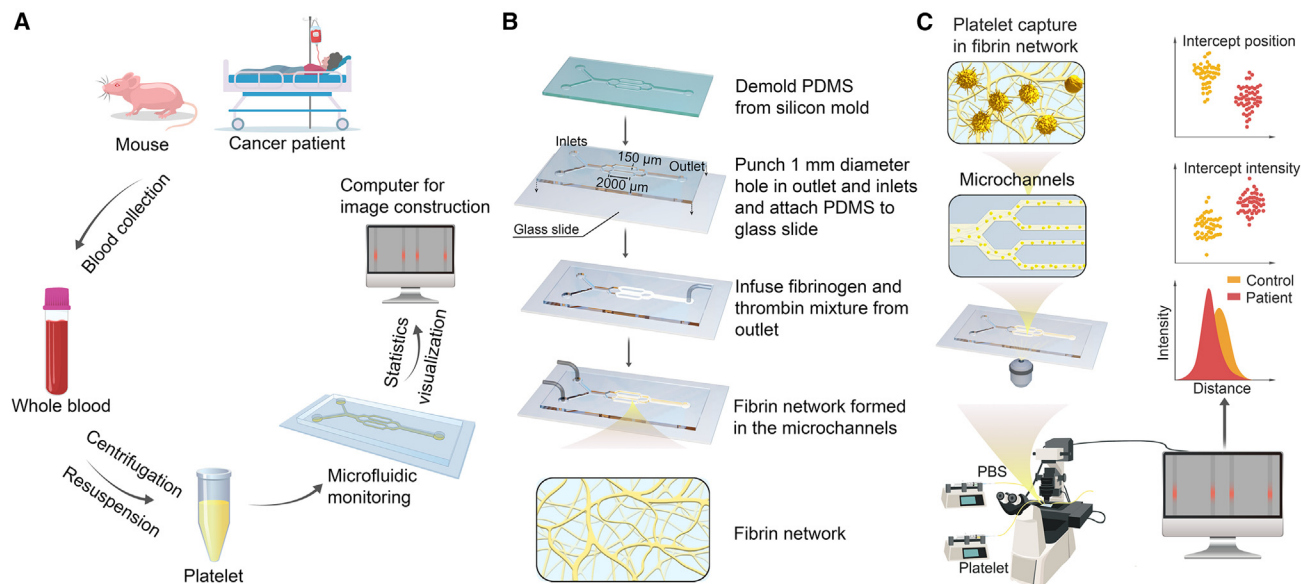


Figure 1. Schematic illustration of sample collection and the working principle of the microfluidic device

(A) Experimental workflow consisting of blood draw, sample preparation, microfluidic detection, and digital image analysis.

(B) Schematic illustration of the fabrication of the device. The microfluidic device was fabricated using polydimethylsiloxane (PDMS), then one outlet and two inlets of approximately 1 mm in diameter were created, of which the outlet was used for perfusing fibrinogen and thrombin to establish the fibrin network in the microchannels, while the inlets were used for inputting platelet samples for the measurement of platelet activity. The thrombin and fibrinogen solutions were mixed (1:1 volume ratio) in an ice bath and stirred gently to prepare the network of fibrinogen. A novel yet relatively simple fabrication process flow enables efficient device manufacture.

(C) Schematic illustration of the fluorescence microscopy setup for image acquisition. Platelet activity status is determined through captured abundance and position via fluorescence microscopy. Each of the top panels, from left to right, shows sequentially magnified views of the capture of hyperactive/activated platelets by the fibrin network in the microchannels.

See also [Figure S1](#).

patient death. Better clinical management and prediction of thrombosis in cancer patients is a real need. Unfortunately, the underlying development of cancer-associated thrombosis remains elusive owing to the lack of specific tools or methods to reliably examine the variation of highly associated clotting markers.

Platelets are anucleate, small (2–4 μm), short-lived (7–10 days) circulating cells in the blood that contribute to physiological hemostasis and pathological thrombus formation by forming aggregates that stop bleeding and initiate coagulation.¹⁶ Beyond these essential functions, many molecular and functional studies in the last decade have shown direct or indirect (e.g., secreted materials from tumor cells) interactions between platelets and tumor cells, resulting in hyperactivity or activation of circulating platelets, all determinately potentiating a thrombotic tendency in cancer patients.¹ More specifically, the incidence of thromboembolic events differs significantly depending on whether the adhesion of hyperactive/activated platelets to fibrin network is sufficiently strong, which is determined by the degree of platelet activation. Thus, precisely measuring the activity changes of peripheral circulating platelets may enable thromboembolic event prediction and subsequent formulation of treatment strategies. Various methods already exist for monitoring platelet activity, such as light transmission aggregometry (LTA), impedance aggregometry, flow cytometry, thromboelastography (TEG), and rotational throm-

boelastometry (ROTEM). However, each technique has drawbacks. LTA and impedance aggregometry are time intensive, necessitate large blood samples, and are affected by pre-analytical variables. Flow cytometry is intricate and requires specialized equipment and expertise. TEG and ROTEM yield limited information on platelet function and are sensitive to pre-analytical variables as well. These limitations emphasize the need for a platelet activity detection device with enhanced sensitivity and accuracy to overcome existing method constraints and offer a more reliable and accessible approach to monitor platelet function.^{17–20} In addition, a major limitation in the current platelet activity testing is the difficulty in replicating biorheological conditions *in vitro*, which incorporate the effects of hemodynamic forces (pressure, flow, and shear stress).

To overcome this limitation and make our measurement more physiologically representative, we developed a fibrin-network-containing microfluidic device that simultaneously measures the affinity of millions of individually circulating platelets for fibrin architecture while sufficiently modeling the dynamic flow in the living vessels. We proceeded to explore the utility of evaluating this binding ability in predicting thrombus complications in clinical cancer patients along with tumor occurrence and development. As seen in [Figure 1A](#), our data-driven analysis method consists of: (1) peripheral blood (1 mL) drawn from tumor-bearing mice or cancer patients; (2) sample preparation by isolating platelets from the blood and performing

fluorescence staining; (3) high-throughput fluorescence imaging of microchannels, as a large population of platelets flow through the fibrin matrix, by high-sensitivity rapid-imaging fluorescence microscopy of a microfluidic device; and (4) digital image processing and the application of various techniques for statistical platelet activity analysis. The device was infused with a stationary phase matrix (fibrin network containing pore sizes from 1 to 5 μm) for subsequent chromatographic testing of a mobile phase (washed platelet suspension). The fibrin network functions as a trap for hyperactive/activated platelets through the interaction between the activated platelet membrane receptor integrin $\alpha\text{IIb}\beta_3$ and fibrin molecules, so as to assess the binding ability of platelets to fibrins during flow-through under shear gradients. The isolated platelets were pre-labeled with dyes to track their position and arrest in the microchannels through microscopic image acquisition. The capture of platelets works similarly to a chromatographic instrument, reflecting the abundance and captured position in the flow channels. Image acquisition and clinical laboratory testing were performed in mice and hospitalized patients with early- and advanced-stage tumors to observe platelet activity status changes associated with tumor progression. The ability of our approach to efficiently differentiate the activity state of platelets from different stages of tumors demonstrates its potential as an independent earlier predictive factor for tumor-associated thrombosis, with much greater accuracy than the conventional blood coagulation parameters, including activated partial thromboplastin time (APTT), thrombin time (TT), fibrinogen (FIB), and prothrombin time (PT), commonly used for evaluating systematic coagulation activity in the clinic. With its simple operation and high sensitivity, the device has the potential for clinical application.

RESULTS

Fabrication and parameter optimization of the microfluidic device

We fabricated the microfluidic device using polydimethylsiloxane (PDMS), which is widely used in applications of soft lithography in biology research because of its excellent biocompatibility, flexibility, insulation, and non-reactivity (Figures 1B and S1A).²¹ One outlet and two inlets of approximately 1 mm in diameter were created, of which the outlet was used for perfusing fibrinogen and thrombin to establish a fibrin network in the microchannels, while the inlets were used for inputting platelet samples and wash buffers (Figure 1B). The four-parallel-channel design was chosen to allow the device to overcome the granularity of responses that can occur in single channel (for example due to occasional passing of debris, air bubbles, or other local perturbations), and provide a more robust global measurement of the systemic level of platelet activity. The end of the fibrin network was set to the site where four parallel channels converge into two flows to avoid unnecessary platelet capture. The infusion of platelets and wash buffers through different inlets avoided replacing lines and needles, thus permitting continuous platelet capture and washing of unbound platelets in the flow process. In addition, the width and length of the observation region (150 μm \times 2,000 μm /each) were designed to fit on a standard, low-magnification field enabling simultaneous real-time

optical microscopic imaging while ensuring near-homogeneous flow in all parallel channels (Figures 1C and S1B).²²

Fibrin network porosity and pore size are crucial parameters in the consistent flow of resting platelets through the microchannels as well as successful arrest of hyperactive/activated platelets. We first optimized the fibrin framework geometry by adjusting the concentration of fibrinogen according to previous studies.^{23,24}

Concentration-dependent experiments suggested that at a fibrinogen concentration of 5 mg/mL, both pore size and fiber thickness reached peak values. This phenomenon can be attributed to the balance between fibrinogen polymerization, crosslinking, and network formation. Although a fibrinogen concentration of 5 mg/mL exhibited peak values for both pore size and fiber thickness, the optimal pore size in each channel was achieved at a 10 mg/mL fibrinogen perfusion (Figures 2A–2E). In this condition, the resting platelets from healthy volunteers can smoothly flow through the channels or be slightly captured at the late position (Figure S1C), whereas hyperactive/activated platelets are captured significantly, due to the expression of membrane receptors binding to fibrin or shape change (i.e., pseudopod and spreading) (Figures 2A and 2B). Increasing concentrations of fibrinogen resulted in smaller pore size with a result of clogging at the beginning of the microchannels when perfused with activated platelets; on the contrary, the decreased concentrations led to lower porosity, making platelets flow through nearly without any interaction with the matrix network. To further exclude the possible influence of experimental process itself on platelet activity, we investigated platelet arrest features under a series of incremental flow rates (from 400 s^{-1} to 1,600 s^{-1}). The results show that platelet arrest levels increased with an increase of flow rate, and the arrested position in the channels occurred earlier (Figures S1D–S1F), indicating that greater shear rates were able to induce more platelet hyperactivity/activation over time. Because platelet arrest abundance started to substantially increase at a flow rate of 1,200 s^{-1} , we selected 1,000 s^{-1} flow rate (one of the typical shear rates in normal arteries) for subsequent experiments, for which image acquisition was performed at a throughput of 60 events per second where an event is defined as an image record. Under this shear rate, the repetitive infusion of resting platelet samples did not stimulate any detectable platelet hyperactivity/activation (Figures S1G and S1H), and repetitive infusion of activated platelets also resulted in similarly captured platelet abundance and position (Figures 2E, S1I, and S1J). These results indicate the performance stability of the device.

Measuring the capture of agonist-activated platelets with the device

We next tested the arrest ability of our fibrin-network-containing microfluidic device for platelets activated by a typically physiologically present platelet agonist, ADP. Washed platelets obtained from the blood of healthy BALB/c nude mice were treated with 10 μM ADP at room temperature and labeled with Cellmask Orange. A suspension of fluorescence-labeled platelets was perfused into the microfluidic channels via one of the inlets at a flow speed of 1,000 s^{-1} . Typical fluorescence images of large populations of platelets show that markedly more platelets

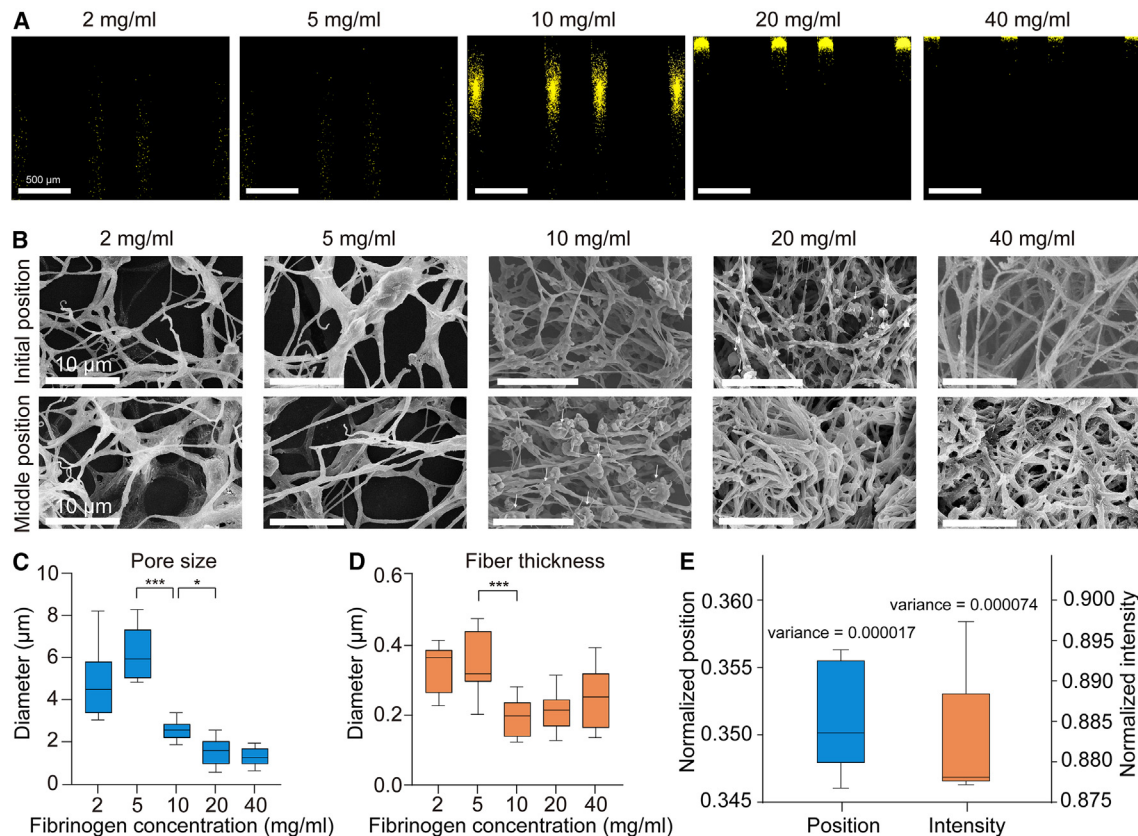


Figure 2. Fibrin concentration dependence of platelet capture

(A) Various fibrinogen concentrations (2, 5, 10, 20, and 40 mg/mL) were used to create fibrin network microenvironments within the microchannels. Thrombin-activated, membrane fluorescence-labeled platelets were then perfused, and the most efficient capture of platelets within the fibrin polymers was observed at a fibrinogen concentration of 10 mg/mL, as demonstrated by the representative fluorescence images of platelets flowing through the channels (yellow color). At fibrinogen concentrations below 5 mg/mL, the fibrin network pores within the microfluidic device are too large for efficient activated platelet capture. In contrast, at fibrinogen concentrations of 20 mg/mL or higher, the fibrin network pores become too small, leading to the complete capture of activated platelets at the initial position. Scale bars, 500 μm .

(B) Scanning electron micrographs suggest that activated platelets efficiently attached to the fibrin framework at 10 mg/mL fibrinogen when flowing through the microchannels. Scale bars, 10 μm .

(C and D) Quantification of pore size (C) and fiber thickness (D) of the fibrin network under the indicated fibrinogen concentrations. * $p < 0.05$, ** $p < 0.01$, and *** $p < 0.001$, one-way ANOVA with Tukey's multiple comparisons test.

(E) Quantification and statistics of platelet capture (intercept position and fluorescence intensity) in five experimental replicates.

Data are depicted as the mean \pm SD.

See also [Figures S1](#) and [S2](#).

were captured in the channels in the ADP treatment groups than in the untreated control group ([Figures S2A–S2E](#)). Specifically, the intercept position of platelets in the microchannels occurred earlier because of ADP treatment, indicating that higher activity of platelets leads to stronger adhesion to the fibrin molecules. Scanning electron microscopy (SEM) images further indicated a markedly greater abundance of captured platelets in the ADP-treated group compared with the control ([Figure S2F](#)). In addition, we discovered that the fibrin network structure remained intact and undamaged, even with platelet adhesion, following a single perfusion of platelet suspension and wash buffer at the tested flow rate ([Figure S2F](#)). This finding indicates the robust stability of these fibrin networks. To confirm whether this observable capturing effect indeed relies on platelet activa-

tion, we pre-treated platelet samples with prostaglandin E₁ (PGE₁, 100 μM), a well-characterized platelet activation inhibitor, before treatment with ADP. PGE₁ pre-treatment significantly abolished the arrest effect of platelets in the channels, as revealed by considerably lower abundance and later intercept position in contrast to the group treated with ADP alone.

We then employed the common flow-cytometry assay to compare its measure of platelet activity with microfluidic device-based measure after treating platelets with agonist in the presence or absence of PGE₁ using antibodies specific for the activated platelet surface markers CD41/CD61 and CD62p. Similar to the results from our device, ADP treatment led to platelet activation to a greater level compared with the untreated control, while pre-treatment with PGE₁ substantially blocked

this activation effect (Figures S2G and S2H). These data confirm the excellent performance of our device at distinguishing platelets exhibiting different activity status via different capture readouts. It is important to note that, although flow cytometry enables the statistical analysis of large populations of particles by evaluating their physicochemical properties by impedance, scattering, or fluorescence measurements under flow, the lack of spatial resolution in flow cytometry limits accurate differentiation between single platelet and platelet microaggregates,²⁵ and hence cannot accurately divulge platelet phenotypic heterogeneity.

Activity measurement of platelets from tumor-bearing mice

Next, we attempted to investigate the signal output when platelets from mice bearing MHCC-97H liver cancer, which has been reported to be strongly associated with DVT occurrence during tumor progression,^{1,26} flowed through our device. Specifically, nearly half of patients with this type of liver tumor develop distal metastases within 1 year of diagnosis with concomitant DVT. As a parallel observation, we also selected a mouse model bearing MDA-MB-231 breast tumors, because DVT occurrence is shown to be less common in breast cancer patients.^{1,2} We separately established early-stage and advanced-stage tumors in both mouse models to better comprehend the transition process of platelet activity over tumor progression. In both cases, the tumors were visible and measurable 1 week after subcutaneous cell inoculation, with a tumor volume of $\sim 150 \text{ mm}^3$. Six weeks later, multiple metastasis foci in the lungs of both mice were detectable, as demonstrated by H&E staining (Figure S3A). We then collected the platelets from the blood of 1 mL of mice bearing inoculating tumor cells, 1-week tumors, and 6-week tumors and performed capture analysis in the microchannels. Interestingly, we detected a significantly greater abundance of captured platelets in the mice with visible solid tumors but not in those bearing 3-day tumor-cell inoculation compared with the healthy control mice (Figures 3A–3G), indicating the gradual presence of hyperactive platelets along with tumor progression. The intercept positions of platelets in the microchannels were also present earlier in samples from solid tumor-bearing mice than in those from other groups (Figures 3A–3G). Furthermore, in both tumor models a significant increase in platelet abundance and a much earlier intercept position were observed in the 6-week tumor groups compared with those bearing 1-week tumors. This is congruent with the clinical reports of tumor patients whose thrombotic risk increases with tumor progression.^{2,27} In addition, the platelets derived from liver tumor-bearing mice were more efficiently captured in the device than those from breast cancer-bearing mice at either visible tumor stage (Figures 3A–3G). This finding is indeed consistent with previous studies indicating that patients with liver cancer have a more increased risk of thromboembolism than those with breast cancer.^{1,2,26}

To confirm the observations of tumor-associated platelet activity from the device, we performed a spreading assay that is particularly useful in characterizing morphological changes and cytoskeletal organization of platelets following activation, although the analysis is manual and tedious.²⁸ Microscopy

data suggest that the platelets derived from mice bearing 6-week liver tumors achieved maximum spreading on fibrinogen-coated surfaces within 6 min (Figure S3B); however, this spreading time was prolonged to 10 and 20 min for platelets of 1-week tumor-bearing mice and the controls, revealing the highest activity degree of platelets in 6-week tumor-bearing mice. In the breast cancer-bearing mice, similar results were found; the full spreading time of platelets from 6-week tumor-bearing mice was 10 min, whereas it was 20 min for the mice bearing 1-week tumors or the controls. These findings reveal a strong positive relationship between degree of tumor progression and the degree of activity of circulating platelets. The data support a high performance of our fibrin-loaded microfluidic device in distinguishing tumor-associated platelet activity state.

To explore the association between platelet hyperactivity and blood system hypercoagulability, we additionally performed conventional clinical laboratory coagulation parameter tests for tumor-bearing mice. As shown in Figures 3H–3K, the APTT and TT were found to be statistically consistent with the platelet hyperactivity measured for the advanced-stage (6-week tumor) liver tumor-bearing mice, as indicated by Spearman's rank correlation coefficients greater than 0.4 for these two parameters (Figures S4A–S4D), whereas the FIB and PT parameters did not correlate with any tumor stage in either tumor type. APTT is an important indicator commonly used to evaluate the activity of the intrinsic blood coagulation pathway. Shortened APTT or TT indicates a hyperactive intrinsic clotting state and/or inhibited fibrinolysis.²⁹ The strong correlation between platelet hyperactivity and APTT/TT demonstrates that platelet hyperactivity can predict abnormal activation of the intrinsic coagulation system and/or activation of fibrinolysis inhibition under severe tumor progression.

Prior studies have shown that tumor occurrence can induce overexpression of tissue factors or generation of tissue-factor-bearing microparticles, resulting in activation of the extrinsic pathway of blood coagulation, which is associated with PT shortening.² However, in our data PT did not significantly correlate with platelet hyperactivity and tumor progression. This unexpected finding may be because the extrinsic pathway is less perturbed than the intrinsic pathway in our established tumor models. In addition, the tumor-progression-dependent increase in platelet activity, as revealed by our microfluidic device, suggests the presence of a non-negligible intrinsic coagulation activation-triggered thrombotic risk that cannot be detected by APTT or TT when in early-stage or non-metastatic tumors. Our results corroborate earlier reports showing that tumor-educated platelets are the first messengers of tumor-associated thrombus events³⁰ and that platelet activation is among the earliest events in the cancer-associated coagulation cascade.^{9,31} Taken together, these data demonstrate that our method exhibits better predictive accuracy for early-cancer-associated thrombotic risk than the conventional coagulation indices; however, it is not directly applicable to tumor screening because we did not detect any change in platelet activity prior to the presence of solid tumors. We further investigated whether antiplatelet drugs may alleviate the excessive activation of platelets induced by cancer. We orally administered clopidogrel, an inhibitor of P2Y₁₂ receptor on the platelet surface, to MHCC-97H or

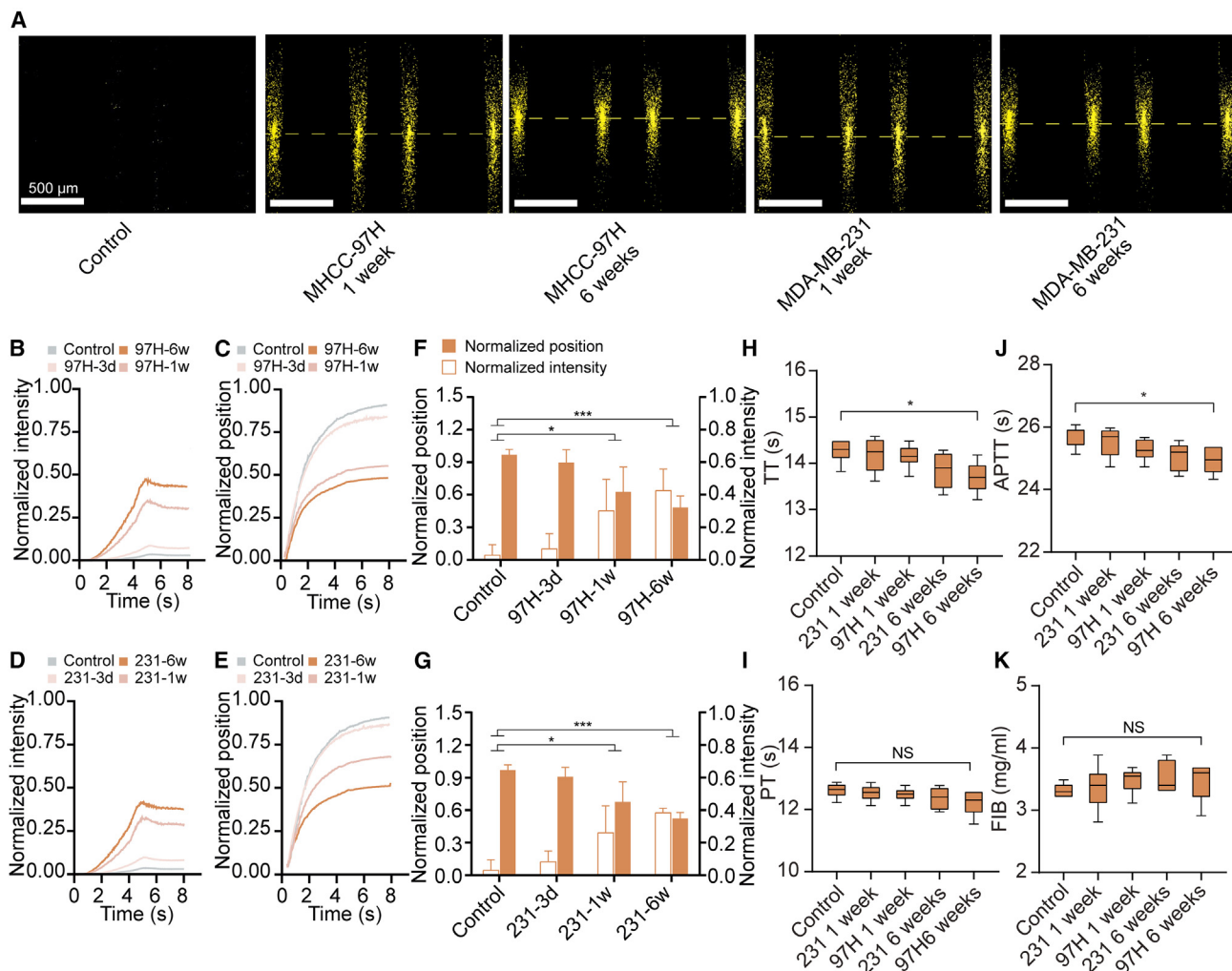


Figure 3. Measuring platelet activity of tumor-bearing mice

(A) Platelets from nude mice bearing different stages of MHCC-97H liver tumors or MDA-MB-231 breast tumors adhere to fibrin networks of the microchannels with a greater abundance than those from the control mice ($n = 6$, biologically independent samples). Areas of intercept position of platelets are indicated with lines, with higher positions indicating greater platelet activity. Scale bars, 500 μm .

(B–E) Changes of platelet abundance (B and D) and intercept position (C and E) in the channels over time. 97H, MHCC-97H liver tumors; 231, MDA-MB-231 breast tumors.

(F and G) Quantification of captured platelet fluorescence intensity and intercept position for MHCC-97H (F) liver and MDA-MB-231 (G) breast cancer models. Data are depicted as the mean \pm SD ($n = 6$, biologically independent samples). * $p < 0.05$, ** $p < 0.01$, and *** $p < 0.001$, one-way ANOVA with Tukey's multiple comparisons test.

(H–K) Conventional coagulation index testing of blood samples from the indicated mouse models, including prothrombin time (PT), activated partial thromboplastin time (APTT), thrombin time (TT), and fibrinogen (FIB). Data are depicted as the mean \pm SD ($n = 6$, biologically independent samples). * $p < 0.05$, ** $p < 0.01$, and *** $p < 0.001$, one-way ANOVA test with Tukey's multiple comparisons test; ns, not significant.

See also [Figures S3](#) and [S4](#).

MDA-MB-231 tumor-bearing mice at a dosage of 10 mg/kg. After providing the medication once daily for seven consecutive days, we isolated platelet samples from various groups of tumor-bearing mice and assessed their coagulation activity using our microfluidic device. Compared with the saline control group, the platelet samples from the clopidogrel-treated group exhibited less capture and lower retention positions within the microfluidic device ([Figure S4E](#)). These results suggest that clopidogrel treatment can effectively alleviate tumor-induced

platelet activation or hypercoagulability, making antiplatelet therapy a promising approach for addressing tumor-related thrombosis.

Measurement of platelet activity in cancer patients and thrombosis prediction potential

To test the performance of our device in measuring platelet activity in clinical cancer patients, we obtained platelet samples from the blood of patients (1 mL/patient) with early lung

cancer (n = 24), advanced lung cancer (n = 25), early liver cancer (n = 27), advanced liver cancer (n = 23), early breast cancer (n = 22), or advanced breast cancer (n = 20). Negative control platelets were obtained from healthy volunteers (n = 20) following the same sample preparation procedure on the same day to minimize potential bias in the microfluidic detection results that may arise from experimental variations in blood draw and storage, sample preparation, platelet quantification, or fluorescence labeling; hence, the *in vivo* state of platelet activity was maintained while the effects of platelet activation *in vitro* were avoided. Overall, our results reveal a greater abundance of captured platelets in the microchannels in the patient groups than in healthy controls (Figures 4A and 4B). Specifically, the platelets from patients with advanced tumors exhibited markedly greater activity compared with those from patients of early-stage tumors, with the maximal arrested value occurring in the group of patients with advanced liver cancer. These findings fit prior reports demonstrating that patients with advanced-stage tumors face greater risk of a thrombotic event than early-stage individuals.^{1,2}

We also evaluated the conventional clinical coagulation parameters in these patients and healthy controls, including PT, TT, APTT, and FIB, and analyzed the association of these parameters with platelet hyperactivity. In the blood of the advanced lung cancer and liver cancer patients, a significant decrease in APTT and TT was present compared with healthy controls (Figures S5A–S5D). In contrast, no significant differences in all four parameters were detected between patients with any type of early-stage tumors and healthy controls (Figures 4C and 4D). Similar to the results of mouse tumor models, APTT and TT were found to be statistically relevant to platelet activity only in the advanced-stage tumor patients, with Spearman's rank correlation coefficients greater than 0.4 for all these parameters (Figures S5E and S5F). The lack of correlation between platelet activity and system coagulation indices in the early-stage patients implies that the activity of circulating platelets can function as an independent factor to predict the potential risk of thrombus formation. These findings suggest that our device is sensitive to platelet activity as a precursor of thrombotic events (TEs) in tumor patients, while the systemic coagulation test is insufficient to predict thrombotic risk unless the severity of patients' tumor progression is high.

To validate whether platelet hyperactivity measured by our device is indeed associated with thrombosis occurrence in cancer patients, we conducted 6 months of clinical follow-up of the tested cancer patients. We categorized the enrolled patients into two groups. The high thrombosis risk group comprised those patients whose captured platelet fluorescent intensity exceeded the upper limit of a 99.99% confidence interval of healthy group, and the low thrombosis risk group comprised those patients whose fluorescent intensity remained below the upper limit of a 99.99% confidence interval of the healthy group. At the end of the follow-up, the incidence rate of TEs, including myocardial infarction, cerebral peduncle, and DVT, in the high-risk group of patients with advanced-stage tumors was 29.6% (16 out of 54, Figure 4E). In contrast, only one detectable thrombotic complication occurred in the low-risk group of 14 patients with advanced-stage tumors. Figure 4F shows the receiver-operating

characteristic (ROC) curve of the captured platelet abundance and conventional coagulation parameters in the advanced-stage tumor patients who developed detectable thrombus symptoms in contrast to advanced-stage tumor patients without TEs. The large value of the area under the curve (AUC) of 0.842 in the ROC curve indicates the excellent performance of the microfluidic device in predicting tumor-associated thrombus disease, in comparison with 0.561, 0.642, 0.564, and 0.686 for TT, APTT, PT, and FIB detection, respectively. In addition, we found that the patient's quality of life was ostensibly better in the low thrombosis risk group, with as much as 34.1% of early-stage patients' tumors in remission and 78.6% of advanced-stage patients' tumors well controlled without further progression. However, 40.7% of advanced-stage patients in the high thrombosis risk group exhibited significant tumor progression with multiorgan metastasis or even death (Figure 4G). The close association between thromboembolism events and poor prognosis was also reflected by a higher TE incidence (40.0%) in advanced-stage tumor patients with adverse outcomes than in those with stable disease (16.3%; Figure S5G). These findings support that the data from our measurements are valuable in predicting the occurrence of TEs in both early- and advanced-stage tumor patients, with high predictive accuracy. Moreover, our findings also suggest that platelet hyperactivity is an effective indicator of poor prognosis and can guide stepped-care case management by frequent monitoring to avoid missing incidences of thrombosis and tumor progression.

High sensitivity in monitoring pulmonary embolism and stroke

To extend the practicability of the microfluidic device, we investigated its potential application in evaluating platelet activity in common acute thrombotic diseases by establishing both pulmonary embolism and brain stroke ischemia-reperfusion mouse models in which microvascular occlusion occurs after middle cerebral artery recanalization, according to methods reported previously by our group (Figures S6A and S6B).³² Our analysis revealed that, compared with healthy control mice, the platelets from thrombosis-bearing mice were captured in the microchannels to a much greater extent (Figures 5A–5D, and S6C), accompanied by the occurrence of an earlier intercepted position (Figures 5A–5C and S6D). The results also suggest a more potent capability of the microfluidic device to discriminate aberrant coagulation status in stroke and pulmonary embolism. The capability of all tests to discriminate hypercoagulability was defined as the ratio of intergroup variation in comparison with the systematic errors of detection methods. These values were 4.11 for stroke mice and 5.67 for pulmonary embolism mice in the intercepted intensity test, and 8.86 for stroke mice and 9.57 for pulmonary embolism mice in the intercepted position test (Figure S6E). Interestingly, unlike the results from tumor-bearing mice, a slight but significant decrease in TT, APTT, and PT coagulation parameters were detected in both thrombosis model mice compared with the control mice (Figures S6F–S6I). The capability of these parameters to discriminate hypercoagulability was calculated to be 1.98 (TT), 1.94 (APTT), and 1.61 (PT) for stroke model mice and 2.62 (TT), 2.48 (APTT), and 2.13 (PT) for pulmonary embolism model mice (Figures S6F–S6I). With

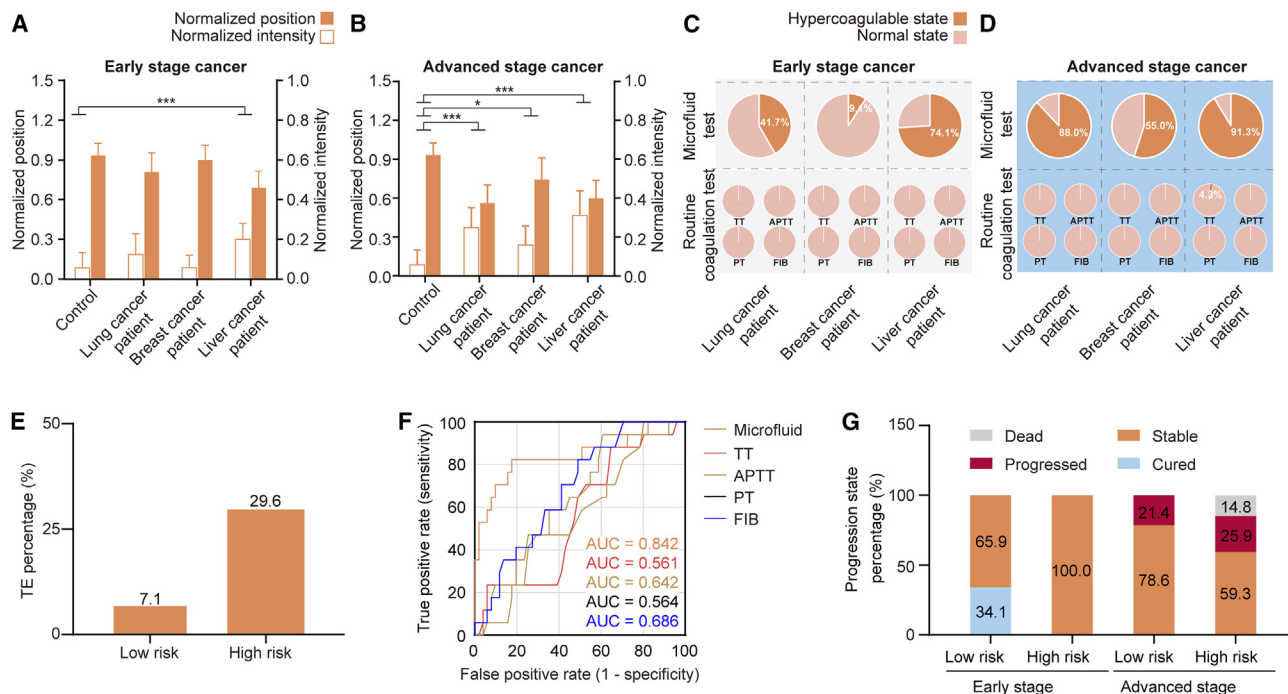


Figure 4. Platelet activity measurement for cancer patients and clinical predictive potential

(A and B) Tumor patient platelets exhibited significantly increased capture in the microchannels compared with those of healthy controls. In some tumor types, platelet abundance was greater in advanced-stage patients than in early-stage patients (healthy control, $n = 20$; early-stage lung cancer, $n = 24$; early-stage breast cancer, $n = 22$; early-stage liver cancer, $n = 27$; advanced-stage lung cancer, $n = 25$; advanced-stage breast cancer, $n = 20$; advanced-stage liver cancer, $n = 23$; biologically independent samples). Data are depicted as the mean \pm SD. * $p < 0.05$, ** $p < 0.01$, and *** $p < 0.001$, one-way ANOVA with Tukey-Kramer multiple comparisons test.

(C and D) Comparison of the coagulation system activation detection rate for patients with different tumor types and stages, as measured with our microfluidic device for platelet activity analysis and clinical laboratory indices including PT, TT, APTT, and FIB for whole blood coagulation status analysis. Our microfluidic device, with its higher resolution, can detect changes in platelet activity in cancer patients more effectively than the commonly used clinical coagulation profile tests.

(E) Correlation between platelet hyperactivity measured using the device and the occurrence rate of thrombotic diseases in patients with advanced tumors (advanced-stage lung cancer, $n = 25$; advanced-stage breast cancer, $n = 20$; advanced-stage liver cancer, $n = 23$; biologically independent samples).

(F) Receiver-operating characteristic (ROC) curve of the device test and conventional coagulation parameters for predicting thromboembolism events in advanced tumor patients during 6-month follow-up (early-stage lung cancer, $n = 24$; early-stage breast cancer, $n = 22$; early-stage liver cancer, $n = 27$; advanced-stage lung cancer, $n = 25$; advanced-stage breast cancer, $n = 20$; advanced-stage liver cancer, $n = 23$; biologically independent samples).

(G) Comparison of tumor progression state in patients with tumors of different thrombosis risks after 6-month follow-up (early-stage lung cancer, $n = 24$; early-stage breast cancer, $n = 22$; early-stage liver cancer, $n = 27$; advanced-stage lung cancer, $n = 25$; advanced-stage breast cancer, $n = 20$; advanced-stage liver cancer, $n = 23$; biologically independent samples).

See also [Figure S5](#).

respect to FIB, in the stroke model the acute endothelial injury and inflammation may induce fibrinogen synthesis at a certain time, but the clot formation in large vessels rapidly consumed fibrinogen in the pulmonary embolism model, resulting in opposite changes in plasma fibrinogen levels in the two thrombus models (Figures S6F–S6I). The positive correlation between platelet hyperactivity/activation and coagulation system activation is indicative of our method's ability to detect the variation in the coagulation system status under venous thrombus or arteriole thrombus formation in the lung or brain. In particular, the higher detection rate and more apparent changes in platelet activity using our method supports that our device has a decidedly greater sensitivity in assaying the activation of the blood coagulation system than conventional coagulation test methods. Thus, individuals who may have developed microthrombi too small to

lead to substantial coagulation system changes may be identified by our method, improving clinical diagnosis for the incidence of TEs.

DISCUSSION

Here we describe a rapid microfluidic approach to measure the activity status of tumor-associated platelets in blood samples and demonstrate the predictive value of platelet hyperactivity/activation for thrombotic complications in cancer patients. Specifically, we found a strongly positive correlation between the degree of activity of circulating platelets and the severity of tumor progression. Platelet activity increased in the early-stage tumor-bearing mice or patients while no detectable variations were apparent using conventional coagulation tests (i.e., APTT,

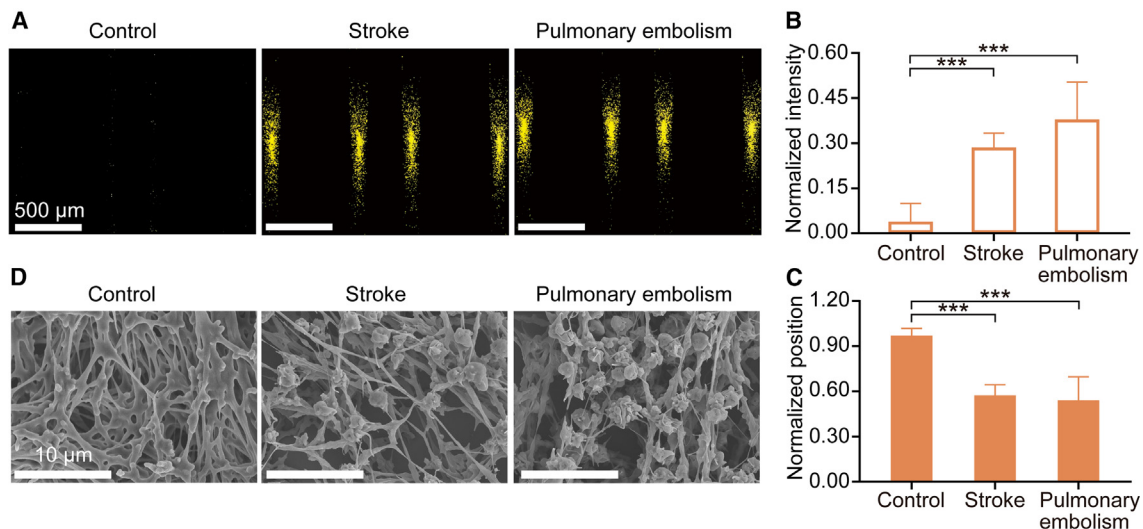


Figure 5. Platelet activity measurements in mice with cardiovascular thrombotic diseases

(A) Platelets from stroke or pulmonary embolism model mice exhibit significant capture in the microchannels compared with those of normal healthy controls ($n = 6$, biologically independent samples). Scale bars, 500 μm .

(B and C) Quantification of captured platelet fluorescence intensity (B) and intercept position (C) for the indicated groups. Data are depicted as the mean \pm SD ($n = 6$, biologically independent samples). * $p < 0.05$, ** $p < 0.01$, and *** $p < 0.001$, one-way ANOVA with Tukey's multiple comparisons test.

(D) Typical SEM images of platelets trapped in the fibrin polymers. Scale bars, 10 μm .

See also Figure S6.

TT, FIB, and PT). Thus, our method is highly sensitive to the activation of the blood coagulation system as a potential precursor of thrombus formation in cancer patients, whereas the conventional coagulation parameters are insensitive to it unless the severity of tumor progression is already high. These findings are also congruous with previous reports that platelets are hyperactive in cancer patients, not just via activator induction (e.g., ADP, thrombin, serotonin) but also via the direct contact effect with tumor cells,^{1,2} which may account for the anomalous presence of hyperactive platelets but no detectable changes in other coagulation markers in the individuals with early-stage tumor in our study. Our 6-month follow-up data of the advanced-stage cancer patients verify the positive link between the hyperactivity of circulating platelets and the risk of thrombotic complications. In particular, the high AUC in the ROC curve of the captured platelets in the advanced-stage tumor patients indicates that both the sensitivity and specificity of our method are high.

Our findings suggest that measuring the activity state of circulating platelets is a potentially effective approach to predict the potential risk of earlier thrombus events in cancer patients, a condition for which no specifically predictive method has been developed so far. In our study, platelet hyperactivity/activation was found to be closely involved in the development process of tumors; timely antiplatelet therapy may be effective in decreasing the incidence of TEs and improving clinical outcomes in cancer patients. Besides this, our microfluidic device offers several advantages over other existing technologies, making it a superior option for detecting platelet activation and assessing cancer or thrombotic diseases. Its improved sensitivity enables more accurate assessments, while its

time-efficient measurement process is particularly suitable for clinical settings. Designed with ease of use in mind, operation is facile with minimal possibility for user error, ensuring consistent results across different users and laboratories. Moreover, the device is constructed from cost-effective components to provide an accessible option without compromising measurement quality, making it an ideal solution for both researchers and clinicians.

Limitations of study

There are several limitations to our study. First, all participating patients were hospitalized patients at the Chinese PLA General Hospital and Fourth Hospital of Hebei Medical University, which may have introduced a selection bias; multicenter studies are needed to draw more general conclusions. Second, our method is not directly applicable to tumor diagnosis/screening because hyperactive platelets were only identified in mice bearing visible solid tumors and because platelet hyperactivity may occur under other pathological conditions. Moreover, although a strong relationship between platelet hyperactivity and thrombotic diseases has also been observed in other animal disease models (e.g., pulmonary embolism and stroke ischemia-reperfusion), validation of circulating platelet activity in patients needs to be performed. Strikingly, numerous studies have demonstrated extensive diffuse microthrombi within peripheral capillaries and arterioles in lungs, heart, and other organs of COVID-19 patients, resulting in multiorgan failure, which is the primary cause of patient death.^{33,34} A prospective study might be needed to determine whether platelet activity change measured by our device can predict the development of microthrombi in COVID-19 infectious

individuals. With these additional studies, our method may hold promise for predicting thrombosis incidence in an early-stage tumor and for developing treatment strategies for preventing TEs and tumor progression in patients in general.

STAR★METHODS

Detailed methods are provided in the online version of this paper and include the following:

- **KEY RESOURCES TABLE**
- **RESOURCE AVAILABILITY**
 - Lead contact
 - Materials availability
 - Data and code availability
- **EXPERIMENTAL MODEL AND STUDY PARTICIPANT DETAILS**
 - Cell lines
 - Animal experiments
 - Ethics approvals and clinical patient eligibility criteria
- **METHOD DETAILS**
 - Microfluidic device fabrication
 - Stationary protein gelation
 - Preparation of platelet samples
 - Biological chromatography
 - Scanning electron microscopy
 - Quantification and visualization of microfluidics results
 - Real-time platelet spreading assay
 - Flow cytometry
 - Analysis of traditional blood coagulation indicators
 - Statistical analysis

SUPPLEMENTAL INFORMATION

Supplemental information can be found online at <https://doi.org/10.1016/j.crmeth.2023.100513>.

ACKNOWLEDGMENTS

This work was supported by grants from the Beijing Distinguished Young Scientist program (JQ20037), the National Natural Science Foundation of China (31730032, 31820103004, 31728007, 81871489, 91859118), the Strategic Priority Research Program of the Chinese Academy of Sciences (XDB36000000), CAS Interdisciplinary Innovation Team (JCTD-2020-04), and Key Area Research and Development Program of Guangdong Province (2020B0101020004).

AUTHOR CONTRIBUTIONS

B. L., Z. L., and Z. Y. contributed equally to this work. S.L. and G.N. designed the research. B.L., Z.L., and Z.Y. performed the experiments. All authors analyzed and interpreted the data. S.L., B.L., Z.L., and G.N. wrote the manuscript.

DECLARATION OF INTERESTS

The authors declare no competing interests.

INCLUSION AND DIVERSITY

We support inclusive, diverse, and equitable conduct of research.

Received: January 13, 2023

Revised: May 3, 2023

Accepted: June 1, 2023

Published: June 27, 2023

REFERENCES

1. Buller, H.R., van Doormaal, F.F., van Sluis, G.L., and Kamphuisen, P.W. (2007). Cancer and thrombosis: from molecular mechanisms to clinical presentations. *J. Thromb. Haemostasis* 5, 246–254. <https://doi.org/10.1111/j.1538-7836.2007.02497.x>.
2. Timp, J.F., Braekkan, S.K., Versteeg, H.H., and Cannegieter, S.C. (2013). Epidemiology of cancer-associated venous thrombosis. *Blood* 122, 1712–1723. <https://doi.org/10.1182/blood-2013-04-460121>.
3. Gussoni, G., Frasson, S., La Regina, M., Di Micco, P., and Monreal, M.; RIETE Investigators (2013). Three-month mortality rate and clinical predictors in patients with venous thromboembolism and cancer. Findings from the RIETE registry. *Thromb. Res.* 131, 24–30. <https://doi.org/10.1016/j.thromres.2012.10.007>.
4. Heit, J.A., O'Fallon, W.M., Petterson, T.M., Lohse, C.M., Silverstein, M.D., Mohr, D.N., and Melton, L.J., 3rd. (2002). Relative impact of risk factors for deep vein thrombosis and pulmonary embolism: a population-based study. *Arch. Intern. Med.* 162, 1245–1248. <https://doi.org/10.1001/archinte.162.11.1245>.
5. Imberti, D., Agnelli, G., Ageno, W., Moia, M., Palareti, G., Pistelli, R., Rossi, R., and Verso, M.; MASTER Investigators (2008). Clinical characteristics and management of cancer-associated acute venous thromboembolism: findings from the MASTER Registry. *Haematologica* 93, 273–278. <https://doi.org/10.3324/haematol.11458>.
6. Naess, I.A., Christiansen, S.C., Romundstad, P., Cannegieter, S.C., Rosendaal, F.R., and Hammerström, J. (2007). Incidence and mortality of venous thrombosis: a population-based study. *J. Thromb. Haemostasis* 5, 692–699. <https://doi.org/10.1111/j.1538-7836.2007.02450.x>.
7. Blom, J.W., Doggen, C.J.M., Osanto, S., and Rosendaal, F.R. (2005). Malignancies, prothrombotic mutations, and the risk of venous thrombosis. *JAMA* 293, 715–722. <https://doi.org/10.1001/jama.293.6.715>.
8. Cronin-Fenton, D.P., Søndergaard, F., Pedersen, L.A., Fryzek, J.P., Cetin, K., Acquavella, J., Baron, J.A., and Sørensen, H.T. (2010). Hospitalisation for venous thromboembolism in cancer patients and the general population: a population-based cohort study in Denmark, 1997–2006. *Br. J. Cancer* 103, 947–953. <https://doi.org/10.1038/sj.bjc.6605883>.
9. Hisada, Y., and Mackman, N. (2017). Cancer-associated pathways and biomarkers of venous thrombosis. *Blood* 130, 1499–1506. <https://doi.org/10.1182/blood-2017-03-743211>.
10. Navi, B.B., Reiner, A.S., Kamel, H., Iadecola, C., Okin, P.M., Elkind, M.S.V., Panageas, K.S., and DeAngelis, L.M. (2017). Risk of arterial thromboembolism in patients with cancer. *J. Am. Coll. Cardiol.* 70, 926–938. <https://doi.org/10.1016/j.jacc.2017.06.047>.
11. Bromberg, M.E., Konigsberg, W.H., Madison, J.F., Pawashe, A., and Garen, A. (1995). Tissue factor promotes melanoma metastasis by a pathway independent of blood coagulation. *Proc. Natl. Acad. Sci. USA.* 92, 8205–8209. <https://doi.org/10.1073/pnas.92.18.8205>.
12. Grignani, G., and Maiolo, A. (2000). Cytokines and hemostasis. *Haematologica* 85, 967–972.
13. Belting, M., Ahamed, J., and Ruf, W. (2005). Signaling of the tissue factor coagulation pathway in angiogenesis and cancer. *Arterioscler. Thromb. Vasc. Biol.* 25, 1545–1550. <https://doi.org/10.1161/01.ATV.0000171155.05809.bf>.
14. Ott, I., Fischer, E.G., Miyagi, Y., Mueller, B.M., and Ruf, W. (1998). A role for tissue factor in cell adhesion and migration mediated by interaction with actin-binding protein 280. *J. Cell Biol.* 140, 1241–1253. <https://doi.org/10.1083/jcb.140.5.1241>.

15. Sorensen, B.B., Rao, L.V.M., Tornehave, D., Gammeltoft, S., and Petersen, L.C. (2003). Antiapoptotic effect of coagulation factor VIIa. *Blood* 102, 1708–1715. <https://doi.org/10.1182/blood-2003-01-0157>.
16. Gaertner, F., and Massberg, S. (2019). Patrolling the vascular borders: platelets in immunity to infection and cancer. *Nat. Rev. Immunol.* 19, 747–760. <https://doi.org/10.1038/s41577-019-0202-z>.
17. Born, G.V. (1962). Aggregation of blood platelets by adenosine diphosphate and its reversal. *Nature* 194, 927–929. <https://doi.org/10.1038/194927b0>.
18. Cardinal, D.C., and Flower, R.J. (1980). The electronic aggregometer: a novel device for assessing platelet behavior in blood. *J. Pharmacol. Methods* 3, 135–158. [https://doi.org/10.1016/0160-5402\(80\)90024-8](https://doi.org/10.1016/0160-5402(80)90024-8).
19. Michelson, A.D. (1996). *Flow cytometry: a clinical test of platelet function.* *Blood* 87, 4925–4936.
20. Sorensen, B., and Ingerslev, J. (2004). Thromboelastography and recombinant factor VIIa-hemophilia and beyond. *Semin. Hematol.* 41, 140–144. <https://doi.org/10.1053/j.seminhematol.2003.11.024>.
21. Nagy, M., Heemskerk, J.W.M., and Swieringa, F. (2017). Use of microfluidics to assess the platelet-based control of coagulation. *Platelets* 28, 441–448. <https://doi.org/10.1080/09537104.2017.1293809>.
22. Jain, A., Graveline, A., Waterhouse, A., Vernet, A., Flaumenhaft, R., and Ingber, D.E. (2016). A shear gradient-activated microfluidic device for automated monitoring of whole blood haemostasis and platelet function. *Nat. Commun.* 7, 10176. <https://doi.org/10.1038/ncomms10176>.
23. Zhao, H., Ma, L., Zhou, J., Mao, Z., Gao, C., and Shen, J. (2008). Fabrication and physical and biological properties of fibrin gel derived from human plasma. *Biomed. Mater.* 3, 015001. <https://doi.org/10.1088/1748-6041/3/1/015001>.
24. Wolberg, A.S. (2007). Thrombin generation and fibrin clot structure. *Blood Rev.* 21, 131–142. <https://doi.org/10.1016/j.blre.2006.11.001>.
25. Nishikawa, M., Kanno, H., Zhou, Y., Xiao, T.H., Suzuki, T., Ibayashi, Y., Harmon, J., Takizawa, S., Hiramatsu, K., Niita, N., et al. (2021). Massive image-based single-cell profiling reveals high levels of circulating platelet aggregates in patients with COVID-19. *Nat. Commun.* 12, 7135. <https://doi.org/10.1038/s41467-021-27378-2>.
26. Lee, A.Y.Y., and Levine, M.N. (2003). Venous thromboembolism and cancer: risks and outcomes. *Circulation* 107, I17–I21. <https://doi.org/10.1161/01.CIR.0000078466.72504.AC>.
27. Khorana, A.A., and Connolly, G.C. (2009). Assessing risk of venous thromboembolism in the patient with cancer. *J. Clin. Oncol.* 27, 4839–4847. <https://doi.org/10.1200/JCO.2009.22.3271>.
28. Aslan, J.E., Itakura, A., Gertz, J.M., and McCarty, O.J.T. (2012). Platelet shape change and spreading. *Methods Mol. Biol.* 788, 91–100. https://doi.org/10.1007/978-1-61779-307-3_7.
29. Deguchi, H., Banerjee, Y., Elias, D.J., and Griffin, J.H. (2016). Elevated CETP lipid transfer activity is associated with the risk of venous thromboembolism. *J. Atherosclerosis Thromb.* 23, 1159–1167. <https://doi.org/10.5551/jat.32201>.
30. Haemmerle, M., Stone, R.L., Menter, D.G., Afshar-Kharghan, V., and Sood, A.K. (2018). The platelet lifeline to cancer: challenges and opportunities. *Cancer Cell* 33, 965–983. <https://doi.org/10.1016/j.ccell.2018.03.002>.
31. Suzuki-Inoue, K. (2019). Platelets and cancer-associated thrombosis: focusing on the platelet activation receptor CLEC-2 and podoplanin. *Blood* 134, 1912–1918. <https://doi.org/10.1182/blood.2019001388>.
32. Xu, J., Zhang, Y., Xu, J., Liu, G., Di, C., Zhao, X., Li, X., Li, Y., Pang, N., Yang, C., et al. (2020). Engineered nanoplatelets for targeted delivery of plasminogen activators to reverse thrombus in multiple mouse thrombosis models. *Adv. Mater.* 32, e1905145. <https://doi.org/10.1002/adma.201905145>.
33. Zhai, Z., Li, C., Chen, Y., Gerotziakas, G., Zhang, Z., Wan, J., Liu, P., Elalamy, I., and Wang, C.; Prevention Treatment of VTE Associated with COVID-19 Infection Consensus Statement Group (2020). Prevention and treatment of venous thromboembolism associated with coronavirus disease 2019 infection: a consensus statement before guidelines. *Thromb. Haemostasis* 120, 937–948. <https://doi.org/10.1055/s-0040-1710019>.
34. Ali, M.A.M., and Spinler, S.A. (2021). COVID-19 and thrombosis: from bench to bedside. *Trends Cardiovasc. Med.* 31, 143–160. <https://doi.org/10.1016/j.tcm.2020.12.004>.
35. Li, B., Chu, T., Wei, J., Zhang, Y., Qi, F., Lu, Z., Gao, C., Zhang, T., Jiang, E., Xu, J., et al. (2021). Platelet-membrane-coated nanoparticles enable vascular disrupting agent combining anti-angiogenic drug for improved tumor vessel impairment. *Nano Lett.* 21, 2588–2595. <https://doi.org/10.1021/acs.nanolett.1c00168>.
36. Li, B., Zhang, X., Wu, Z., Chu, T., Yang, Z., Xu, S., Wu, S., Qie, Y., Lu, Z., Qi, F., et al. (2022). Reducing postoperative recurrence of early-stage hepatocellular carcinoma by a wound-targeted nanodrug. *Adv. Sci.* 9, e2200477. <https://doi.org/10.1002/advs.202200477>.
37. Blum, P., Pircher, J., Merkle, M., Czermak, T., Ribeiro, A., Mannell, H., Krotz, F., Hennrich, A., Spannagl, M., Koppel, S., et al. (2017). Arterial thrombosis in the context of HCV-associated vascular disease can be prevented by protein C. *Cell. Mol. Immunol.* 14, 986–996. <https://doi.org/10.1038/cmi.2016.10>.
38. Psaila, B., Bussel, J.B., Linden, M.D., Babula, B., Li, Y., Barnard, M.R., Tate, C., Mathur, K., Frelinger, A.L., and Michelson, A.D. (2012). In vivo effects of eltrombopag on platelet function in immune thrombocytopenia: no evidence of platelet activation. *Blood* 119, 4066–4072. <https://doi.org/10.1182/blood-2011-11-393900>.

STAR★METHODS

KEY RESOURCES TABLE

REAGENT or RESOURCE	SOURCE	IDENTIFIER
Antibodies		
anti-CD41/CD61	Emfret	RRID:AB_2833084
anti-CD62P	BioLegend	RRID:AB_1979549
Biological samples		
Blood from liver cancer patients	Chinese People's Liberation Army General Hospital	S2016-098-1
Blood from other cancer patients	Fourth Hospital of Hebei Medical University	2021098
Chemicals, peptides, and recombinant proteins		
Polydimethylsiloxane	Dow Corning	Sylgard 184
thrombin	Solarbio	T8020-1000
fibrinogen	HARVEYBIO	9001-32-5
PGE1	Aladdin	P129960
CellMask Orange	Invitrogen	C10045
Critical commercial assays		
PT (prothrombin time) liquid kit	Nanjingxinfan biology	XFS853
APTT (activated partial thrombin time) liquid kit	Nanjingxinfan biology	XFS852
TT (thrombin time) liquid kit	Nanjingxinfan biology	XFS850
FIB (Fibrinogen) liquid kit	Nanjingxinfan biology	XFS849
Deposited data		
The code used for microfluidic image processing in this study	https://github.com/SupingLab/microfulid	https://doi.org/10.5281/zenodo.7992790
Experimental models: Cell lines		
MHCC-97H	Mingzhou Biotech Co., Ltd	MZ-2834
MDA-MB-231	ATCC	HTB-26
Experimental models: Organisms/strains		
BALB/c nude	Vital River	401
Software and algorithms		
GraphPad Prism v8.3.1	GraphPad software	N/A
SPSS Statistics 20	SPSS software	N/A
Processing 3.0 software.	Processing	N/A

RESOURCE AVAILABILITY

Lead contact

For additional information or requests regarding resources and reagents, please direct them to our lead contact, Suping Li (lisuping@nanocr.cn).

Materials availability

The devices developed in this study can be obtained through the [lead contact](#) upon request.

Data and code availability

- All data reported in this paper will be shared by the lead contact upon request.
- All original code has been made publicly available as of the date of publication and can be found at <https://github.com/SupingLab/microfulid>, including the linked repositories therein. An archival DOI is available in the [key resources table](#).
- Any additional information required to reanalyze the data reported in this paper is available from the [lead contact](#) upon request.

EXPERIMENTAL MODEL AND STUDY PARTICIPANT DETAILS

Cell lines

The human liver cancer cell line MHCC-97H (purchased from Mingzhou Biotech Co., Ltd) and human breast cancer cell line MDA-MB-231 (purchased from ATCC) were cultured in DMEM medium (Wisent, Canada) supplemented with 10% fetal bovine serum (FBS) (Wisent, Canada) and 1% Penicillin/Streptomycin (Wisent, Canada).

Animal experiments

4- to 6-week-old female BALB/c nude mice were purchased from Vital River Animal Laboratories. The mice were kept in a SPF animal room for three days before any experiments. In order to construct the subcutaneous tumor-bearing mouse models, 2×10^6 MHCC-97H or MDA-MB-231 cells were suspended in a 100 μ L pre-chilled Matrigel/PBS mixture at a volume ratio of 1:1 and inoculated into female BALB/c nude mice. We monitored the tumor volume using Vernier calipers. At the experimental endpoint, the tumor-bearing mice were euthanized and the organs were collected (including tumor tissues) for further study. All animal experiments were performed according to protocols approved by The National Center for Nanoscience and Technology Animal Care and Use Committee (protocol number, NCNST-LX-2103-44).

Ethics approvals and clinical patient eligibility criteria

Prior to participation, all patients signed an informed consent form. Clinical blood samples were obtained from upper limb veins of patients with histologically confirmed clinical cancer. The blood samples of breast cancer patients all come from the Fourth Affiliated Hospital of Hebei Medical University and the protocol was approved by the Ethics Committees of Hebei Medical University (protocol number, 2021098). The blood samples of patients with other types of tumors all came from the First Medical Center of the General Hospital of the People's Liberation Army and the protocol was approved by the Ethics Committees of Chinese PLA General Hospital (protocol number, S2016-098-01). The patient age ranged from 18 to 70 years old. Notably, all of the breast cancer patients were female. As for the patients with other types of tumors, we ensured gender balance by maintaining an equal number of male and female patients. The Eastern Cooperative Oncology Group (ECOG) performance status of all patients was 0–3 and their expected survival was greater than six months. All patients were staged according to the TNM guidelines. In breast cancer patients, “early stage” refers to the patients with tumor size ≤ 20 mm (T1), no regional metastases (N0) and no clinical or imaging evidence of distant metastases (M0); “advanced stage” refers to the patients that have tumors with metastases at distant sites (Any T, any N, M1). In the lung cancer patients, “early stage” refers to the patients with tumor size ≤ 3 cm (T1), no regional metastases (N0) and no clinical or imaging evidence of distant metastases (M0); “advanced stage” refers to the patients with tumor size > 7 cm (T4) bearing distal metastasis (T4, any N, M1). In the liver cancer patients, “early stage” refers to the patients with solitary tumor ≤ 2 cm, without vascular invasion (T1), no regional metastases (N0) and no clinical or imaging evidence of distant metastases (M0); “advanced stage” refers to the patients that bear tumors with metastases at distant sites (Any T, any N, M1). Patients who received radiation therapy or chemotherapy within six months before our study or had other serious medical illness, prior malignancies or uncontrolled infection were excluded.

METHOD DETAILS

Microfluidic device fabrication

The microfluidic devices presented in this study were fabricated using polydimethylsiloxane (PDMS) (Sylgard 184, Dow Corning) through soft lithography techniques. A silicon master was created with the SU-8 2000 series negative photoresist via photolithography. A PDMS prepolymer was made at a 10:1 ratio of dimer to curing agent and then casted on a silanized master with positive relief of the channel features made by the SU-8 photoresist board. The PDMS was cured at 100°C in a convection oven for 1 h. After curing, the PDMS was gently peeled off the master, followed by oxygen plasma bonding to the microfluidic slide using a plasma cleaner (Harrick Plasma, PDC-32G). The inlets and outlets of the device were then punched through the channels.

Stationary protein gelation

0.1 U/ml thrombin and different concentrations of fibrinogen solutions (2, 5, 10, 20, and 40 mg/mL) were prepared. The microfluidic channel was washed once, thoroughly with ethanol, followed by three washes with PBS. All microfluidic channels were then aspirated completely to remove excess liquid. The thrombin and fibrinogen solutions were mixed (1:1 vol ratio) on an ice bath and stirred gently, to avoid instant gelation, using a pipette tip. The mixture was injected into the microfluidic tunnel inlet with a syringe pump at a rate of 1 mL/min or slower on an ice bath until the liquid level arrived at the inner turn of the observation channel. Note that the mixing time and injection time could not exceed 3 min. If the mixing (fibrinogen and thrombin) and injection time takes too long, the fibrin network may not distribute evenly throughout the microfluidic channel, and may block the front end of the chip. Any excess solution outside the channel was wiped away to ensure a clean and dry device. The gel-filled device was finally incubated at 37°C for 1 h and then freeze dried overnight prior to injecting platelet samples.

Preparation of platelet samples

For acquiring the platelets from mice, whole blood was collected from mice via the orbital sinus and transferred into 1.5 mL polypropylene centrifuge tubes. ACD anti-coagulation buffer (2.2% D-glucose, 1.64% citric acid, 2.85% sodium citrate, 2 μ M PGE1, pH 7.4) was added to the samples at a ratio of nine parts whole blood to one part ACD. To avoid contamination with blood cells, the samples were centrifuged at 200 $\times g$ for 20 min and the platelet-rich plasma (PRP) supernatant layer was transferred into new 1.5 mL centrifuge tubes containing 100 μ L PGE1 (2 μ M). The samples were centrifuged at 1000 g for 10 min and the supernatant, platelet-poor plasma (PPP) layer was gently removed. The sedimented platelets were then gently resuspended in 1 mL modified Tyrode's buffer (12 mM NaHCO₃, 138 mM NaCl, 5.5 mM glucose, 2.9 mM KCl, 2 mM MgCl₂, 0.42 mM NaH₂PO₄, 10 mM HEPES, 2 μ M PGE1 pH = 7.4) which was then centrifuged at 1000 g for 10 min^{35,36}. The platelets were then stained with CellMask Orange (diluted 1:3000) for 15 min at 37°C. After that, the cells were gently washed thrice with modified Tyrode's buffer to remove excess dye solution. Platelet samples labeled with fluorescent dye were counted and adjusted to the final platelet concentration of 2 $\times 10^8$ /mL. The purified platelets were kept at room temperature for no longer than 4 h before use for microfluidic devices analysis. To analyze the therapeutic effects of antiplatelet drugs on tumor-related thrombosis, MHCC-97H or MDA-MB-231 tumor-bearing mice were orally administered clopidogrel, an inhibitor of P2Y₁₂ receptor on platelet surface at a dosage of 10 mg/kg for seven consecutive days, then platelet samples were isolated from various groups of tumor-bearing mice and assessed their coagulation activity using our microfluidic device. To acquire *in vitro* activated platelet samples, 10 μ M ADP solution and 2 U/ml thrombin was added to the platelet samples from healthy mice for exactly 20 min at room temperature.^{37,38}

For acquiring human platelet samples, human blood was donated from healthy volunteers or tumor patients in 10% (v/v) ACD buffer. The blood was first centrifuged at 1100 rpm for 11 min and the platelet-rich plasma (PRP) supernatant layer was transferred to another new tube and centrifuged at 3200 rpm for 3 min. The supernatant was carefully discarded and the pellet was resuspended in modified Tyrode's buffer. The platelets were then stained with CellMask Orange (diluted 1:3000) for 15 min at 37°C. After that, the cells were gently washed thrice with modified Tyrode's buffer to remove excess dye solution. Platelet samples labeled with fluorescent dye were counted and adjusted to the final platelet concentration of 2 $\times 10^8$ /mL. The purified platelets were kept at room temperature for no longer than 4 h before use in microfluidic devices analysis.

Biological chromatography

The microfluidic device was placed onto the stage of a microscope. Using a 5 \times objective, the position of the device was adjusted to achieve an observation field with an area of 976 μ m \times 736 μ m. The collected platelet solution was passed through the microfluidic channel via a syringe pump (Harvard Apparatus) for 4 s at 1000 s⁻¹ from one of the two inlets. The PBS elution solution was then passed through the other inlet for 4 s at 1000 s⁻¹ to remove excess and non-adhesive platelets. When injecting the samples and PBS, images were captured via software at a rate of no lower than 60 FPS. The outlets were connected to a waste container to avoid the exiting sample liquid from covering the observation region and causing signal noise. Vigorous injection was avoided to prevent any liquid leakage or damage to the device due to high pressure.

Scanning election microscopy

After passed through platelet samples, the PDMS layer was cut in a direction vertical to the observation channel. The split samples were then fixed with 2.5% glutaraldehyde in 0.1 M sodium cacodylate buffer for 1 h, followed by washing with PBS. Incremental concentrations of ethanol were applied for 30 min to 1 h. Finally, the samples were freeze dried for 24 h before SEM observation. Fibrin clot morphology and density were assessed using ImageJ software.

Quantification and visualization of microfluidics results

A java footscript was created to integrate the intercept position (P) and fluorescence intensity (I) of the final elution position of each group. Each frame was extracted from the videos and the corresponding position and intensity were visualized. For image acquisition, analysis and data presentation, 200 equalized time-interval frames of each 8 s video (4 s injection +4 s elution) were extracted to perform time-lapse visualization. The internal image analysis and statistical methods were based on pixel counting of fluorescence brightness from the stained platelets. Since each imaged platelet contained numerous pixels, the number of platelets could not be established as a meaningful variable. Thus, the total pixels accumulated during the test were normalized and set to represent the total amount of platelets. For samples whose platelets cannot be detected, the fluorescent intensity was defined as 0 and the intercepted position was defined as 1. The java footscript was designed to execute on Processing 3.0 software.

Real-time platelet spreading assay

Glass coverslips were thoroughly cleaned with isopropanol and dried under a stream of N₂. To fabricate a complete and uniform fibrin coating, the coverslips were activated in a plasma cleaner (Plasma Cleaning, PDC-32 G, Harrick Plasma, Ithaca, NY, USA). 10 μ g/mL fibrinogen and 0.1 U/ml thrombin (1:1 vol ratio) solution (150 μ L total) were added to the coverslips, which were then incubated at room temperature for 1 h to facilitate complete attachment. The coverslips were then washed three times with PBS. For the assay, the coverslips were loaded into the imaging chamber and 200 μ L Tyrode's buffer (138 mM NaCl, 12 mM NaHCO₃, 5.5 mM glucose, 2.9 mM KCl, 1 mM CaCl₂, 1 mM MgCl₂, 1 mM EDTA, 0.36 mM NaH₂PO₄, 0.2% bovine serum albumin, pH = 7.4) was pipetted onto the coverslips. The microscope was set to bright field mode and the coverslips were placed onto the stage. 10 μ L of the platelet

solution from different sources was placed onto the coverslip and the platelet behavior was observed and recorded at 1, 3, 6, 10, and 20 min.

Flow cytometry

To examine the activation level of platelets, platelet surface markers after different treatments or from different sources were analyzed. The platelets were incubated with anti-CD41/CD61 antibody or anti-CD62P mouse recombinant antibody for 20 min at room temperature. Afterward, the platelets were washed three times with PBS and resuspended in PBS for flow cytometry analysis (BD Accuri C6 flow cytometer, BD, USA).

Analysis of traditional blood coagulation indicators

The blood coagulation indicators of the mice were tested using a PT (prothrombin time) liquid kit, TT (thrombin time) liquid kit, APTT (activated partial thrombin time) liquid kit, and FIB (Fibrinogen) liquid kit on a semi-automatic coagulation analyzer (LG-PABER-I, Taizhou, China). The blood coagulation indicators from human volunteers were acquired from the Fourth Hospital of Hebei Medical University and Chinese PLA General Hospital.

Statistical analysis

SPSS 19.0 software was used to perform statistical analysis. Significant differences were assessed by one-way ANOVA with Tukey's or Tukey-Kramer multiple comparisons test or Student's *t* test. Correlation analyses were conducted by two-side Spearman's rank correlation test. **p* < 0.05, ***p* < 0.01, ****p* < 0.001.